International Workshop on Land Use/Cover Changes and Air Pollution in Asia
4-7 August 2015
IPB ICC, Bogor, Indonesia

An Analysis of Aerosol Optical Properties During Seasonal Monsoon Circulation

Lim Hwee San and Sim Chong Keat

hslim@usm.my

School of Physics

Universiti Sains Malaysia

Outline

- Introduction
- Objectives
- Methodology
- Results and Discussions
- Conclusion
- Acknowledgement

Introduction

- Air quality issues in Asia can be attributed to unavoidable climate change impacts and the negative impact of anthropogenic activities arising from rapid population growth, industrialization and urbanization.
- Aerosol optical depth (AOD) derived from remote sensing has potential for assessing air quality.
- Southeast Asia (SEA) stands out globally as it hosts one of the most complex meteorological and environmental conditions, making remote sensing difficult both for AERONET and satellites.
- Development of an empirical model to produce reliable AOD estimates for aerosol monitoring at local scales is novel and necessary for SEA, with potential global applications.

Objective

- To develop an AOD prediction model based on three types of measured data, namely (i) Relative humidity (RH), (ii) Visibility (Vis) and (iii) air pollution index (API).

- To study the optical properties of aerosols in Penang, Malaysia for four monsoonal seasons (northeast monsoon, pre-monsoon, southwest monsoon, and post-monsoon) based on data from the AErosol Robotic NETwork (AERONET) from February 2012 to November 2013.

Methodology

- The present work was based on previous studies of Tan et al. (2014a, b). They predicted AOD using multiple regression analysis based on meteorological and air quality data.
- The AOD prediction model has been validated and successfully proven for the southwest monsoon period (June–September 2012) in Penang Island, Malaysia.
- The first data subset was used to calibrate for AOD at 500 nm, given below:

$$\mathrm{AOD} = a_0 + a_1(\mathrm{RH}) + a_2(\mathrm{RH})^2 + a_3(\mathrm{RH})^3 + a_4(\mathrm{Vis}) + a_5(\mathrm{Vis})^2 + a_6(\mathrm{Vis})^3 + a_7(\mathrm{API}) + a_8(\mathrm{API})^2 + a_9(\mathrm{API})^3$$

RH is the surface relative humidity

Methodology

- The contribution of RH to the aerosol properties was integrated in the aerosol model of Srivastava et al., (2012), because the net effect of RH on aerosol and related factors were difficult to quantify. In similar spirit, the RH contribution is disregarded in the present model, yielding given as follows:

$$\mathrm{AOD} = a_0 + a_1(\mathrm{Vis}) + a_2(\mathrm{Vis})^2 + a_3(\mathrm{Vis})^3 + a_4(\mathrm{API}) + a_5(\mathrm{API})^2 + a_6(\mathrm{API})^3$$

Results and Discussion

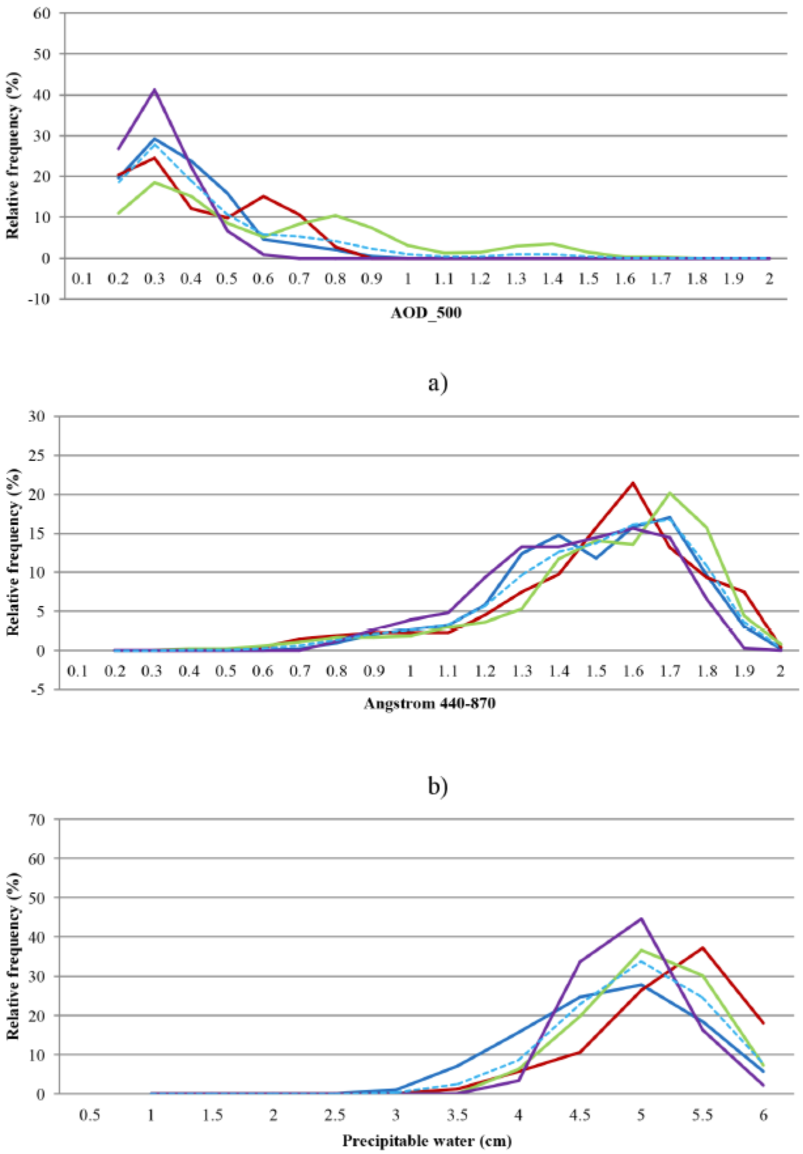

Seasonal variations of AOD, Angstrom exponent, and Precipitable water based on frequency distribution patterns

Figure 1. Seasonal relative frequencies of occurrences of **(a)** AOD_500, **(b)** Ångström440-870, and **(c)** PW in Penang for February 2012 to November 2013. Each curve was smoothed by using a moving average technique.

Results and Discussion

Seasonal discrimination of aerosol types based on the relationship between AOD and Ångström exponent

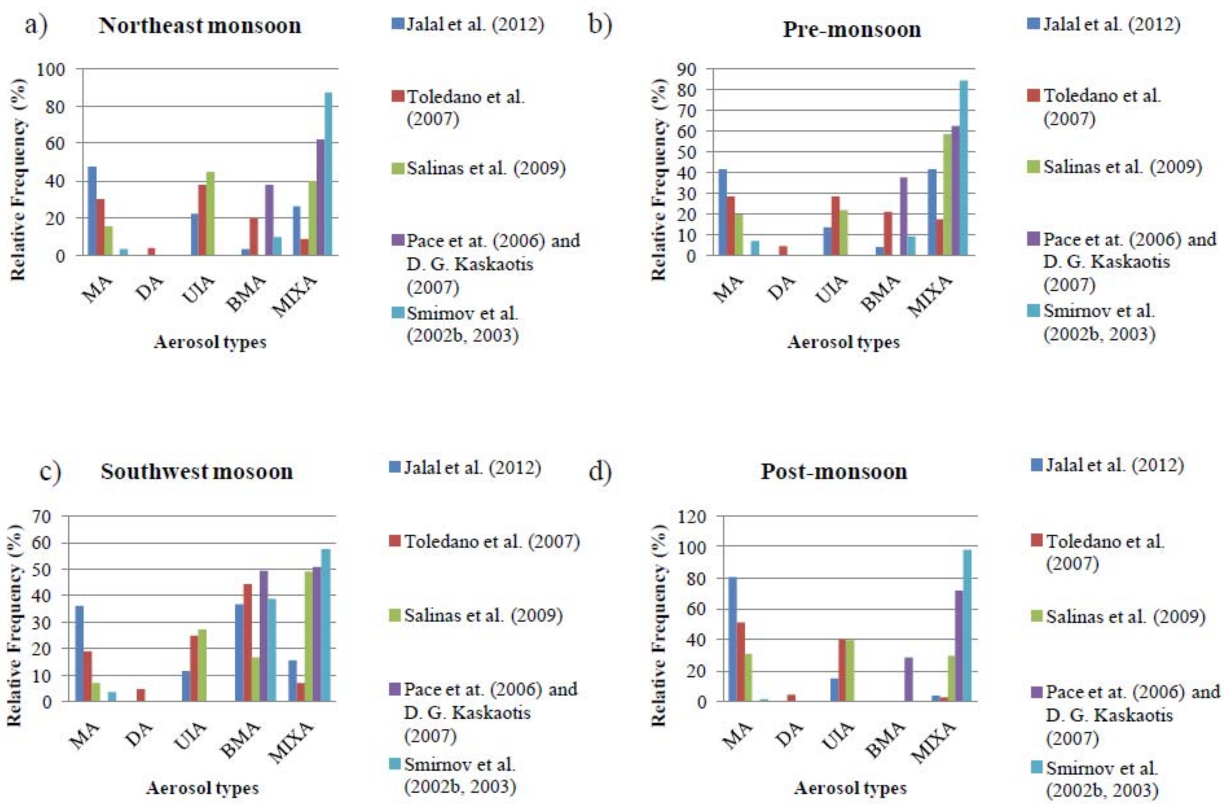

Figure 2. Classification of aerosol types for **(a)** northeast monsoon, **(b)** pre-monsoon, **(c)** southwest monsoon, and **(d)** post-monsoon based on AOD–Ångström440-870 scatter plots by proposed thresholds.

Results and Discussion

Seasonal discrimination of aerosol types based on the relationship between AOD and Ångström exponent

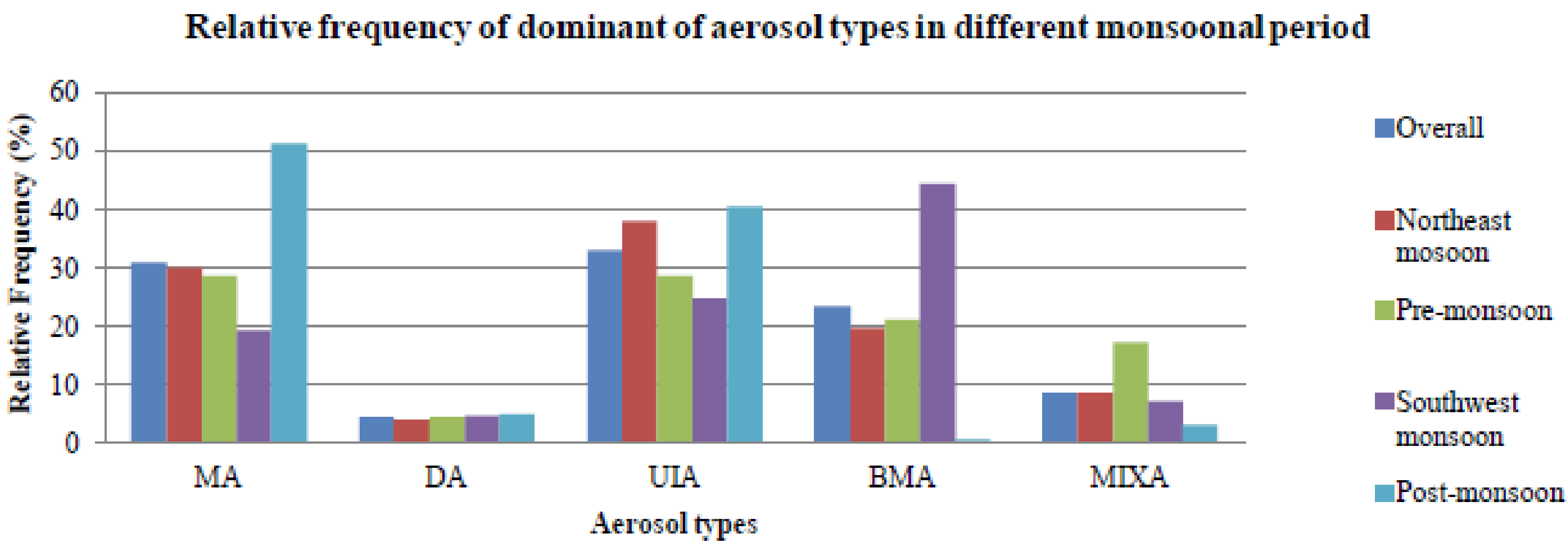

Figure 3. Seasonal classification of aerosol types based on AOD–Ångström440-870 scatter plots by the threshold proposed by Toledano et al. (2007).

Results and Discussion

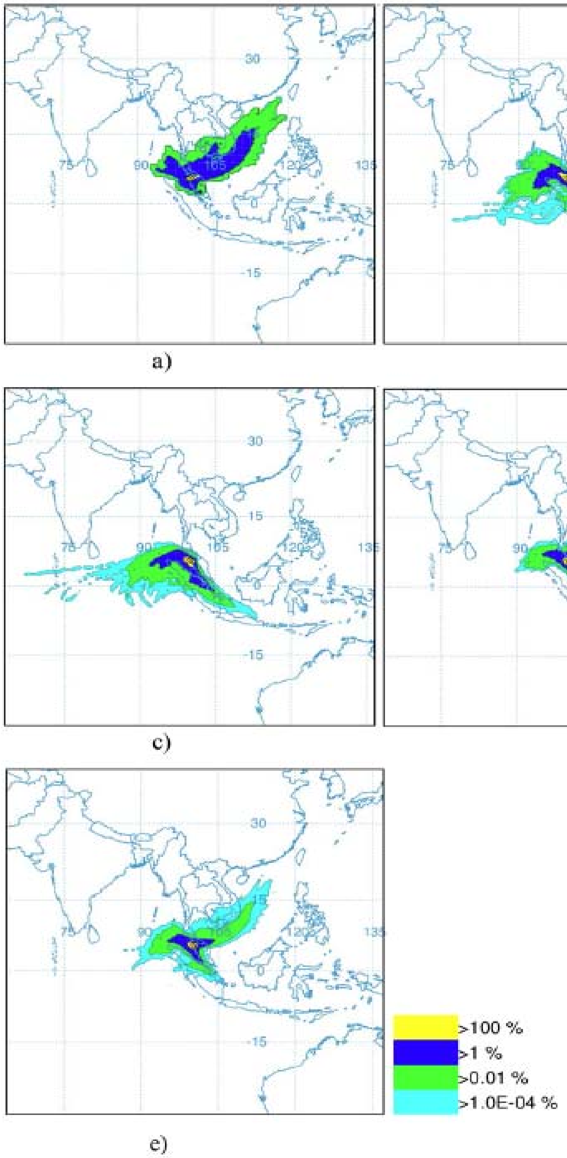

Seasonal flow patterns of air parcels from the HYSPLIT_4 model for identification of aerosol origins

Figure 4. Seasonal back-trajectory frequency plot by the HYSPLIT_4 model (Draxler and Hess, 1998) for (a) northeast monsoon,(b) pre-monsoon, (c) southwest monsoon, (d) post-monsoon, and (e) overall study period at Penang, which was marked as a five edged star (5.50 N and 100.50 E, from altitude 51 m).

Results and Discussion

Examination of predicted AOD values

Table 3. Calibration results (data for subset 1) for the AOD prediction model (Eq. 2) from 2012 and 2013 data.

Monsoon	R^2	RMSE	wMAPE (%)	N
Northeast monsoon	0.41	0.11	0.40	129
Pre-monsoon	0.64	0.11	0.37	65
Southwest monsoon	0.77	0.17	0.08	117
Post-monsoon	0.42	0.06	0.21	83
Overall	0.72	0.13	0.04	394
$\text{Overall}_{\text{POR}}$	0.92	0.06	0.13	307

Note: POR = potential outliers removed, N = number of data

Results and Discussion

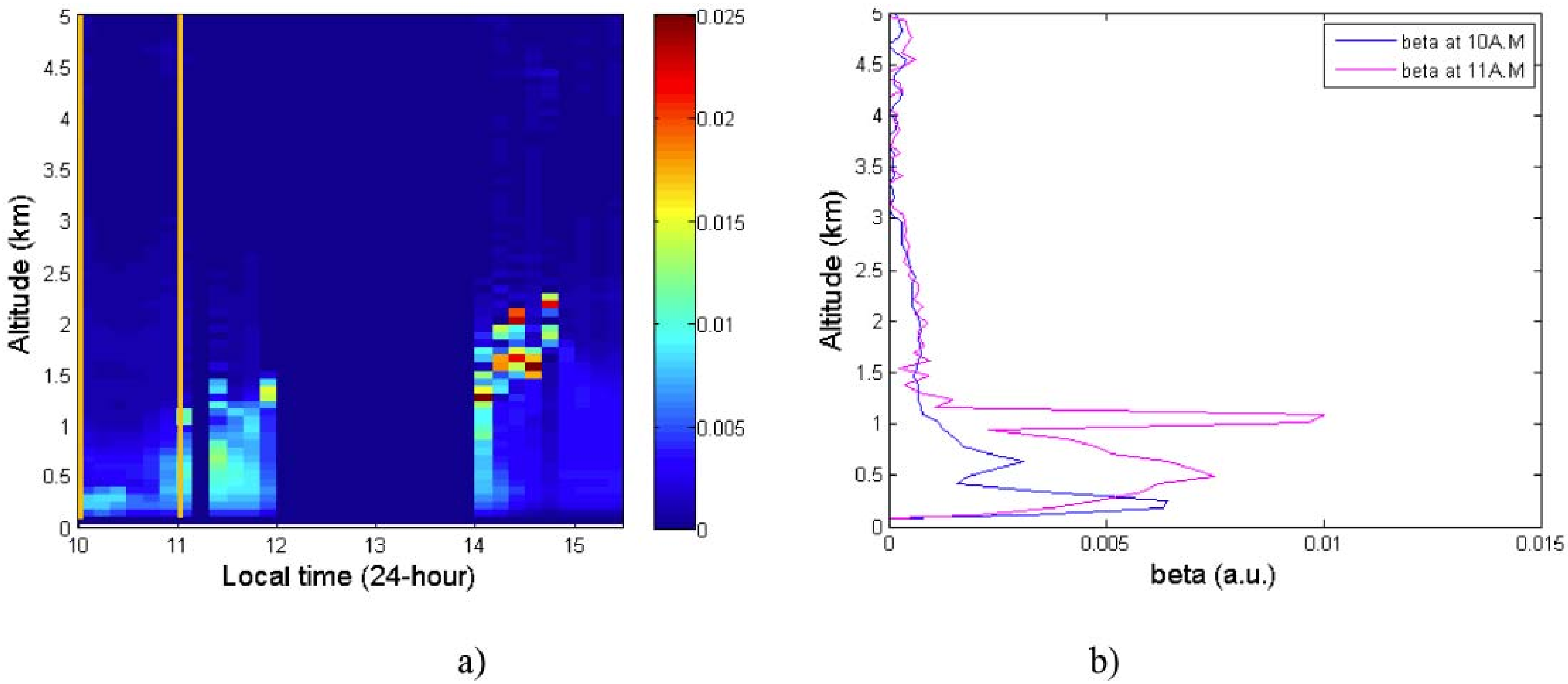

Figure 5. (a) Profiles of the aerosol backscatter coefficients recorded on 12 July 2013. No data were acquired from 12 to 2 p.m. The brown lines represent the moment of acquisition of sun photometer; **(b)** profiles of the aerosol backscatter coefficient (beta) obtained from 10 to 11 a.m. for the brown lines in **(a)**.

Results and Discussion

Applications of the proposed model in the absence of measured AOD data

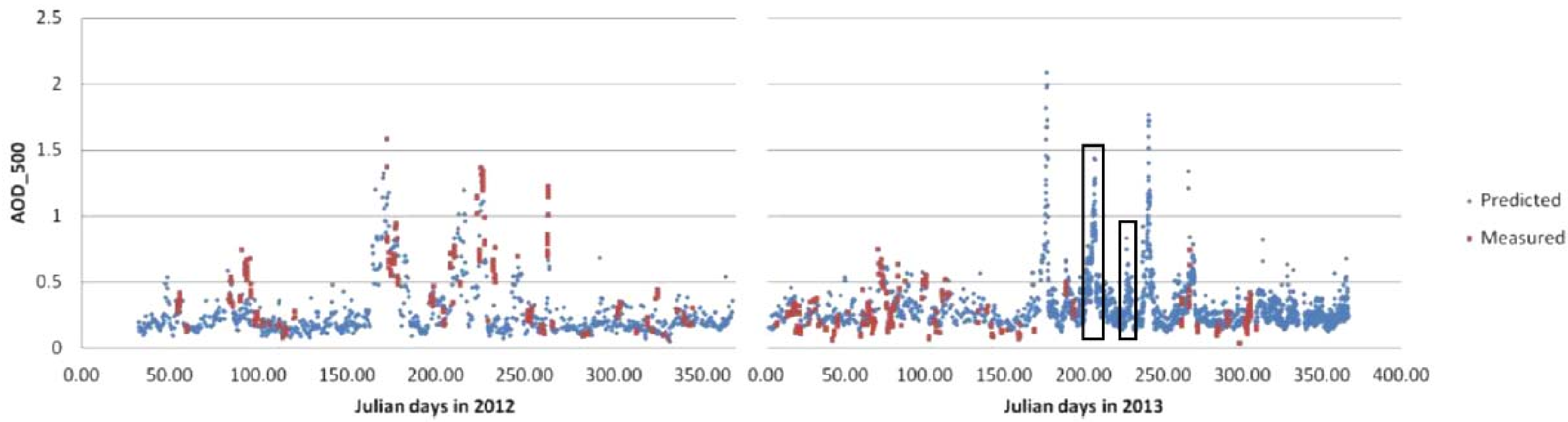

Figure 6. Predicted AOD_500 data plotted against the period from 2012 to 2013 (input all Vis and API available data into the established model to predict AOD, with 4493 data points). Rectangles 1 and 2 correspond to the data recorded on 24–25 July and 13–14 August 2013, respectively. These data were used for comparison with those obtained from LIDAR.

Results and Discussion

Table 1. R2 values of the AOD predicted by selected linear regression models from the literature. The values of R2, RMSE and wMAPE shown in this table are obtained by comparing the predicted AOD values against measured AOD data from subset 1.

Model	Author(s)	R^2	RMSE	wMAPE (%)
$AOD = a_0 + a_1(Vis)$	Retalis et al. (2010)	0.56	0.17	0.08
$AOD = a_0 + a_1(b_{ext})$	Mahowald et al. (2007)	0.58	0.17	0.07
$AOD = a_0 + a_1(PM_{10})$	Gao and Zha (2010), Chen et al. (2013)	0.60	0.16	0.05
$AOD = a_0 + a_1(Vis) + a_2(Vis)^2 + a_3(Vis)^3 + a_4(API) + a_5(API)^2 + a_6(API)^3$	Current Study	0.72	0.13	0.05

Results and Discussion

Comparison with other linear regression models

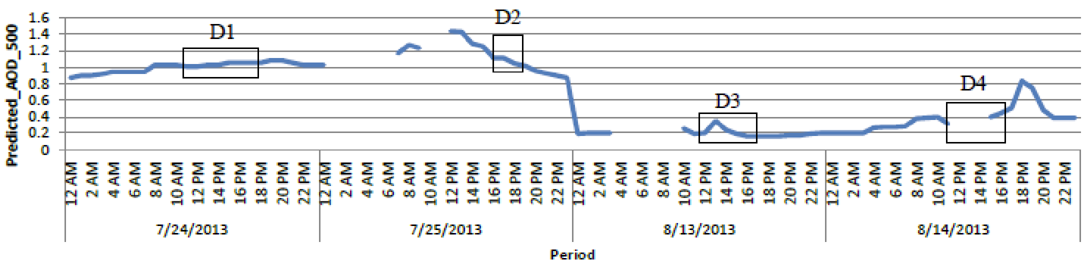

a)

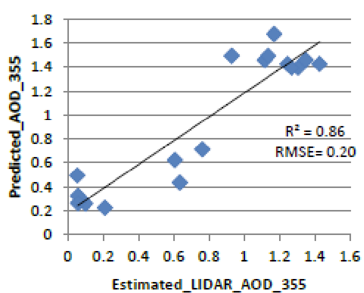

b)

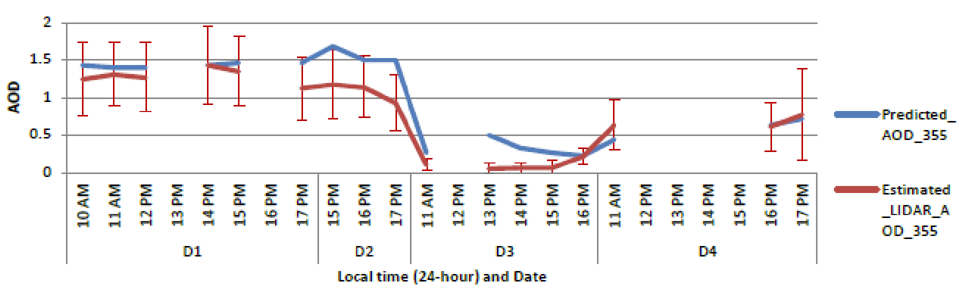

c)

Figure 8. (a) Hourly retrieved AOD recorded on **(a)** 24–25 July and 13–14 August 2013 (the gaps are due to fog, rain, or when API value is predominantly caused by O3 but not PM10/. **(b)** A scatter plot for AOD_355 predicted from our model versus the AOD calculated from Raymetrics LIDAR system. **(c)** Predicted AOD from our model and estimated AOD from LIDAR plotted versus local time and date (the gaps indicate no data available at the particular time due to LIDAR system was switched off or cloud contamination above the LIDAR system). Error bars for estimated AOD from LIDAR are shown.

Conclusion

- For the study period, biomass burning aerosols (BMA) abruptly increased during the southwest monsoon period, because of active open burning activities in local areas and neighbouring countries.
- During the northeast monsoon period, the optical properties (e.g., size distribution patterns) of the aerosols were unique.
- Two noticeable peaks were observed in the occurrence frequency of the Angstrom exponents compared with the single peaks for other monsoon seasons.

Conclusion

- Our algorithm predicts AOD data during non-retrieval days caused by the frequent occurrence of clouds in the equatorial region.
- The proposed model yields reliable near real-time AOD data despite the availability of the measured data for limited time points.
- The predicted AOD data are beneficial for monitoring aerosols in short-term and long-term scenarios, their behaviour, and provides supplementary information for climatological studies and monitoring aerosol variation.

Acknowledgement

This research was supported by

Universiti Sains Malaysia Research University Grant (1001/PFIZIK/811228)

and

Fundamental Research Grant (203/PFIZIK/6711349).

Thank you

Presented by
CK Sim | School of Physic, USM, Malaysia